JBC RESEARCH ARTICLE

Oxidation of two cysteines within yeast Hsp70 impairs proteostasis while directly triggering an Hsf1-dependent cytoprotective response

Received for publication, April 21, 2022, and in revised form, August 16, 2022 Published, Papers in Press, August 27, 2022,
https://doi.org/10.1016/j.jbc.2022.102424

Alec Santiago[1,2] **and Kevin A. Morano**[1,*]

From the [1]*Department of Microbiology and Molecular Genetics, McGovern Medical School at UTHealth Houston, Houston, Texas, USA;* [2]*MD Anderson UTHealth Graduate School of Biomedical Sciences at UTHealth Houston, Houston, Texas, USA*

Edited by Ursula Jakob

Neurodegenerative diseases such as Alzheimer's, Parkinson's, and Huntington's diseases affect millions of Americans every year. One factor linked to the formation of aggregates associated with these diseases is damage sustained to proteins by oxidative stress. Management of protein misfolding by the ubiquitous Hsp70 chaperone family can be modulated by modification of two key cysteines in the ATPase domain by oxidizing or thiol-modifying compounds. To investigate the biological consequences of cysteine modification on the Hsp70 Ssa1 in budding yeast, we generated cysteine null (cysteine to serine) and oxidomimetic (cysteine to aspartic acid) mutant variants of both C264 and C303 and demonstrate reduced ATP binding, hydrolysis, and protein folding properties in both the oxidomimetic and hydrogen peroxide–treated Ssa1. In contrast, cysteine nullification rendered Ssa1 insensitive to oxidative inhibition. Additionally, we determined the oxidomimetic *ssa1-2CD* (C264D, C303D) allele was unable to function as the sole Ssa1 isoform in yeast cells and also exhibited dominant negative effects on cell growth and viability. Ssa1 binds to and represses Hsf1, the major transcription factor controlling the heat shock response, and we found the oxidomimetic Ssa1 failed to stably interact with Hsf1, resulting in constitutive activation of the heat shock response. Consistent with our *in vitro* findings, *ssa1-2CD* cells were compromised for *de novo* folding, post-stress protein refolding, and in regulated degradation of a model terminally misfolded protein. Together, these findings pinpoint Hsp70 as a key link between oxidative stress and proteostasis, information critical to understanding cytoprotective systems that prevent and manage cellular insults underlying complex disease states.

Protein molecular chaperones facilitate proper conformational folding of nascent polypeptides, refolding of proteins from a misfolded state, and shuttling of protein substrates marked for degradation to proteolytic machinery. Disruption of proteomic management can result in accumulation of nonfunctional and/or aggregated proteins, which are often implicated in adverse neurological conditions such as Alzheimer's disease, Parkinson's disease, and Huntington's disease (1–3). In both humans and the yeast *Saccharomyces cerevisiae*, a key chaperone group modulating many of these tasks are the cytosolic heat shock protein 70 (Hsp70) chaperone proteins, composed of an amino-terminal nucleotide-binding/ATPase domain (NBD) and a carboxyl-terminal substrate-binding domain (SBD) that communicate through allosteric interactions with assistance from other highly conserved chaperones (Hsp40, which assists in Hsp70/substrate contact; and Hsp110, which assists in nucleotide exchange) in a process termed chaperone cycling (4, 5). These cochaperones serve to regulate the rate of intrinsic nucleotide hydrolysis and substrate binding and release of Hsp70. Binding of a substrate within the SBD, along with stimulation by Hsp40, induces a conformational cascade that accelerates ATP hydrolysis within the NBD (6). ATP binding, hydrolysis, and release (nucleotide cycling) activity thus alters affinity of the SBD for its targets and also modulates the iterative Hsp70 release/binding mechanism that promotes protein folding. *S. cerevisiae* expresses four cytosolic Hsp70s, of which Ssa1 (human homolog HSPA1A) is the most abundant, constitutively expressed homolog. Yeast in addition possesses another constitutively expressed homolog (Ssa2), and two stress-induced homologs (Ssa3/4), whose expression is restricted until exposure to environmental stress (7). However, expression of any one of the four Ssa isoforms is sufficient to allow viability (8, 9).

Reactive oxygen species (ROS) are unstable and highly reactive molecules derived from oxygen, known to be particularly detrimental to lipids, DNA, and proteins (10). ROS are a common byproduct of normal cellular functions and are typically present at low concentrations, but uncontrolled/acute increases in abundance can negatively impact cell physiology (11). Uncontrolled ROS has been implicated as a contributing factor in aging, cancer, and neurodegenerative disease (12, 13). Oxidative stress management is particularly important for protein homeostasis, as evidenced by the vulnerability of proteins at all stages of their life cycle, and especially nascent polypeptides (14). Several chaperones have been found to act as sensors for oxidative stress, triggering downstream events that protect the cell from damage to proteins (15). Because of their variable reactivity, reversibility, and breadth of oxidative

* For correspondence: Kevin A. Morano, kevin.a.morano@uth.tmc.edu.

states, cysteines represent a versatile and useful sensor for cellular redox state (16, 17). Cysteine oxidation of the yeast peroxiredoxin Tsa1 was shown to alter its normal behavior, whereby it switches from a hydrogen peroxide scavenger to a passive "holdase" chaperone, actively recruiting Hsp70/Hsp104 to assist with clearance of misfolded proteins (16). In bacteria, Hsp33 has been shown to contain reactive cysteines that sense oxidative stress, activating substrate-binding capacity for prolonged periods to similarly convert the inactive chaperone into a holdase to prevent substrate aggregation (18). Reactive cysteines also play a key role in the regulatory relationship between Gpx3 and Yap1, the major transcription factor of the oxidative stress response in yeast (19). In mammalian cells, oxidative stress impacts the regulation of the transcription factor Nrf2 by KEAP, a cysteine-rich protein whose oxidation and subsequent degradation enable Nrf2 to induce an oxidative stress response circuit (20, 21).

Cysteines within Hsp70s have been demonstrated to be important for stress defense, spanning various organisms, cellular compartments, and thiol-modifying compounds (22–24). The triterpenoid compound celastrol, used in traditional Chinese medicine to reduce inflammation, is a thiol-modifying compound that was shown to activate the major regulator of the heat shock response (HSR) in yeast, Hsf1 (25). The HSR is a general stress response, activating the transcription of hundreds of downstream genes, because of several types of stress (26). Ssa1 contains two reactive cysteines (C264 and C303), located within the NBD, and nullification of these cysteines *via* serine substitution was shown to abolish Hsf1 reactivity to thiol-modifying compounds and an inability to activate the HSR in response to oxidative stress but not thermal stress (27). Conversely, mimicking cysteine oxidation to a sulfinic acid moiety *via* substitution of both cysteines with aspartic acid resulted in a constitutively hyperactive HSR (27). Recently, we and others characterized the mechanistic repression of Hsf1 by Ssa1 through direct physical interaction, establishing a correlation between Hsp70 functional status and induction of the HSR as an effort to relieve proteotoxic stress (28, 29). However, a definitive relationship between thiol modification of Ssa1, its regulation of the HSR through Hsf1, and downstream effects on general proteostasis remains to be determined.

Modeling thiol oxidation through genetic techniques has allowed several groups to probe the effects of cysteine modification on chaperone proteins without the broad off-target effects of introducing exogenous oxidative compounds. Distinct amino acid substitutions, such as aspartic acid, were used to effectively mimic the steric and electrostatic changes that result from thiol oxidation. Oxidomimetic substitutions in the human-inducible Hsp70 (HSPA1A) resulted in structural changes to the nucleotide-binding pocket of the chaperone, resulting in both enzymatic and functional deficiencies (30). Oxidomimetic mutations also modified the behavior of the endoplasmic reticulum–localized Hsp70 protein binding immunoglobulin protein (BiP) from that of a protein-maturation assisting "foldase" into a less enzymatically active holdase state, where substrates are passively bound without regulated release. This chaperone reprogramming increased cell survival under conditions of oxidative stress but negatively impacted growth under nonstress conditions (31). While increased association of this mutant form of BiP (C63D) with unfolded polypeptide substrates offered a protective effect against oxidative stress, a C63H substitution that mimics the bulkiness but not the charge of a sulfinic acid was shown to have a dominant negative effect in nonstress conditions, likely because of increased holdase activity that prevented proper folding and secretion of proteins (32). The enzymatic effects of mimicked oxidation through amino acid substitution mirror the reductions in nucleotide binding, ATPase activity, and protein refolding seen from exogenously added oxidizing or alkylating compounds (30, 33, 34). In HeLa cells, glutathionylation of Hsp70 cysteines caused aberrations in substrate recognition and binding, again supporting the notion that Hsp70 cysteines are both highly reactive and functionally vulnerable residues (24).

To better understand the roles of C264 and C303 within Ssa1 as oxidative stress sensors and targets, as well as downstream implications of thiol stress on general Ssa1-dependent proteostasis, we undertook a combined biochemical and genetic approach. The dual sulfinic acid mimic Ssa1-2CD (C264D, C303D) was impaired for several critical Hsp70 functions *in vitro*, including nucleotide binding, ATP hydrolysis, and the refolding of chemically denatured protein. Exogenous oxidation of Ssa1 with hydrogen peroxide mirrored the deficiencies of the Ssa1-2CD mutant, but the cysteine-null Ssa1-2CS (C264S, C303S) variant was impervious to exogenous oxidation, confirming cysteines 264 and 303 as the primary relevant sites of oxidative modification. The *ssa1-2CD* mutant was found to exert a dominant negative growth phenotype in cells and was in addition unable to facilitate growth as the sole cytosolic *SSA* isoform. The oxidomimetic *ssa1-2CD* mutant also exhibited reduced ability to maintain general proteostasis *in vivo*, as evidenced by defective folding and refolding of the reporter protein firefly luciferase (FFL)-GFP as well as inability to promote degradation of a chronically misfolded protein. Extending previous work, we demonstrate that Ssa1-2CD failed to associate with Hsf1 and repress its activity under nonstress conditions, resulting in chronic activation of the HSR. Taken together, these results support a model wherein cysteines within the primary constitutive cytosolic Hsp70 chaperone are subject to oxidative modification that not only negatively impacts general proteostasis but also concomitantly engages the HSR to promote a cytoprotective response.

Results

Ssa1 oxidation reduces ATP binding and hydrolysis

The conformational changes between the NBD and SBD that allow Hsp70 chaperones to iteratively bind and release substrate are dependent on allosteric signals from interactions with nucleotide, substrate, and cochaperones. This process was previously shown to be disrupted by exogenous treatment with thiol-reactive compounds (33). The sulfhydryl alkylating

reagent *N*-ethylmaleimide (NEM) negated the ability of yeast Ssa1 to bind ATP-agarose as well as to hydrolyze ATP (34). To continue exploring the Hsp70/nucleotide relationship and to confirm the relevant amino acid targets of oxidative attack, we generated and purified to homogeneity recombinant Ssa1 proteins with the WT sequence, serine substitutions (Ssa1-2CS), or aspartic acid substitutions (Ssa1-2CD) at cysteines 264 and 303 (27, 35) (Fig. S1*A*). Because binding of ATP within the NBD generates an allosteric signal to induce conformational change of Hsp70, we hypothesized that modification of C264 and C303 would alter the ability of Ssa1 to interact with nucleotide. To test this, we first measured nucleotide-binding ability using ATP-agarose chromatography. Purified proteins were incubated with ATP-agarose, followed by several washes and elution with sample buffer and immunoblot. Comparable amounts of Ssa1 (WT) and Ssa1-2CS were eluted from the ATP-agarose beads after incubation, whereas the Ssa1-2CD protein was unable to bind to the same extent (Fig. 1*A*, quantitated in Fig. 1*B*). Exogenous addition of 1 mM hydrogen peroxide prior to incubation with the beads significantly reduced the signal of eluted Ssa1, whereas Ssa1-2CD ATP binding remained low and nearly identical to untreated sample, as averaged over three experiments (Fig. 1*B*). Importantly, Ssa1-2CS retained full ATP-binding capacity regardless of hydrogen peroxide treatment, suggesting that reduced nucleotide binding is a functional consequence of cysteine oxidation.

To assess whether the reduced binding interaction resulted in a downstream change in catalytic activity, we tested the ability of each isolated protein to hydrolyze ATP using a malachite green assay to quantify released phosphate. Akin to nucleotide binding, Ssa1 and Ssa1-2CS exhibited comparable levels of specific activity, whereas Ssa1-2CD demonstrated significantly reduced hydrolysis (Fig. 1*C*). Treatment with hydrogen peroxide also drastically reduced ATP hydrolysis of the Ssa1 but not Ssa1-2CS protein, whereas Ssa1-2CS retained full and even slightly elevated activity. Hydrolysis of ATP in the NBD is stimulated by Hsp40. We therefore wanted to determine if stimulation by Hsp40 could overcome the basal hydrolysis deficit of Ssa1-2CD. Interestingly, the addition of the Hsp40 Ydj1 and the Hsp110 Sse1 equally stimulated all Ssa1 isolates but was not able to rectify the deficiency in hydrolysis from Ssa1-2CD (Fig. S1*B*). Together, these data indicate that modification of cysteines, by both exogenous oxidation and oxidomimetic mutation, results in an altered relationship between Ssa1 and nucleotide resulting in reduced ability to bind and hydrolyze ATP.

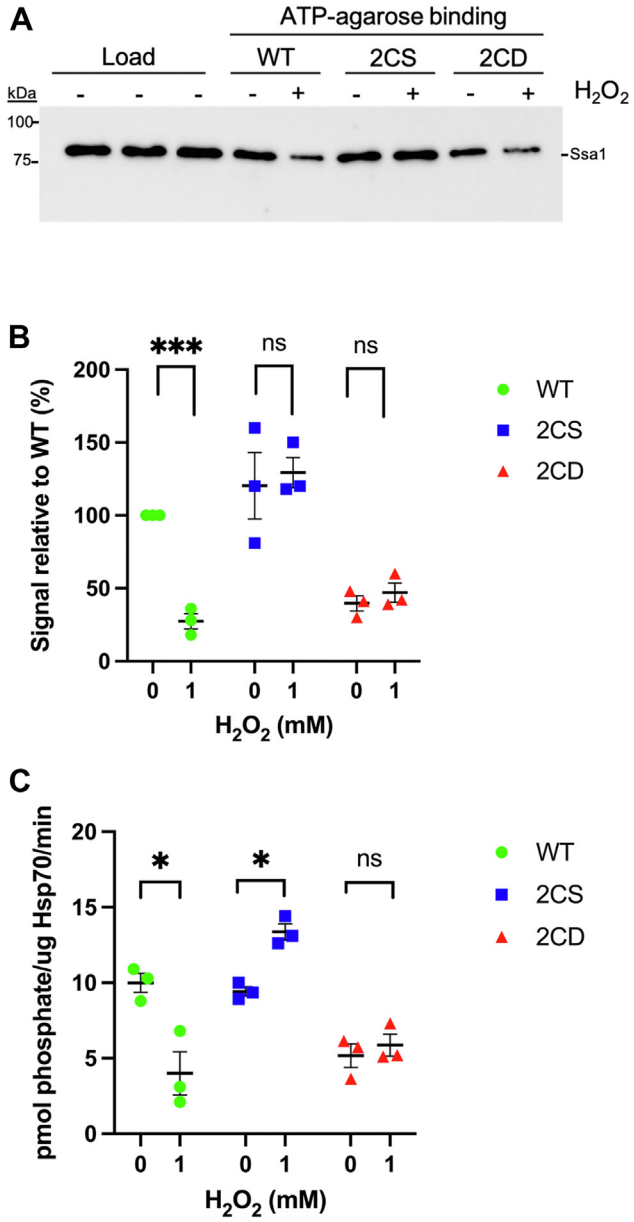

Figure 1. Nucleotide binding and hydrolysis are similarly impaired by oxidomimetic substitution in Ssa1-2CD and exogenous oxidation of Ssa1. *A*, immunoblot displaying elution fraction of 25 μl ATP-agarose bead volume incubated with 1 μM total respective protein treated or not with 1 mM hydrogen peroxide. *B*, quantification of the signal in *A* converted to relative percentage of untreated Ssa1 and normalized for load. *C*, rate of ATP hydrolysis by 0.1 μM of respective proteins, treated or not with 1 mM hydrogen peroxide. *Bolded horizontal bars* indicate mean, and error bars indicate SEM.

Ssa1 oxidation inactivates substrate folding

Disruption of nucleotide interaction within the NBD of Hsp70 has negative implications for the allosteric conformational changes signaled through the linker to the SBD, possibly affecting substrate interaction (36). To assess differential NBD conformational status, we performed limited trypsinization of isolated Ssa1 variants as used previously to interrogate NBD structure by monitoring proteolytic fragmentation patterns of Hsp70 (37). We incubated each chaperone mutant with either ATP or the nonhydrolyzable ATP-γ-S analog, followed by limited trypsin digestion. Interestingly, we observed increased and nucleotide-independent generation of what we believe to be the SBDα "lid" domain in the 2CD mutant based on apparent molecular mass, as compared with WT and 2CS (Fig. S4*A*) (38). We infer that this may be due to 2CD being locked into one conformation for a longer period, stabilizing SBDα in a more exposed state. To determine the consequences of impaired nucleotide interaction on protein folding by Hsp70, we utilized recombinant FFL as a substrate for Ssa1.

Susceptible to chemical denaturation, the enzymatic activity of properly folded FFL to produce chemiluminescence in the presence of the substrate luciferin has been previously used to measure substrate refolding by yeast chaperones *in vitro* (39–41). We therefore reconstituted the Hsp70 folding triad that includes Hsp70 (Ssa1), Hsp40 (Ydj1), and Hsp110 (Sse1) to examine refolding of chemically denatured FFL *in vitro*. Ssa1 and the cysteine-null Ssa1-2CS were found to have comparable basal ability to refold FFL postexposure to guanidinium hydrochloride, whereas the yield of active enzyme produced by Ssa1-2CD was dramatically reduced and refolding without Ssa1 presence was found to be negligible (Fig. 2*A*). The yeast disaggregase Hsp104 assists Hsp70 and Hsp40 in the reactivation of aggregated proteins (42). After addition of this disaggregase to our chaperone mixture, we found that while Hsp104 approximately doubled the final yield of FFL recovered for all strains, there was still a significant defect in folding by Ssa1-2CD as compared with Ssa1-WT and Ssa1-2CS (Fig. 2*B*). To determine the effects of exogenous oxidation on refolding, we measured the final yield of recovered FFL after preexposure of Ssa1 alone to 1 mM hydrogen peroxide and found that there was a significant decrease in recovery by SSA1-WT after oxidation, whereas Ssa1-2CS and Ssa1-2CD interestingly exhibited increased folding with respect to their untreated matched samples (Fig. 2*C*). We hypothesize that this may be due to a secondary effect that shifts the conformation of Ssa1, such as oxidation of cysteine 15 or a previously unidentified methionine residue, but further inquiry is necessary. However, because the observed increases occurred in both the serine and aspartic acid mutants, these effects are likely independent of cysteines 264 and 303. We also attempted to recover the refolding abilities of WT after exogenous oxidation by treatment with the reductant DTT. We did not observe significant restoration of refolding, possibly because of hyperoxidation state of the thiol moiety by hydrogen peroxide to a sulfinic acid or a sulfonic acid, the former of which is genetically modeled by the 2CD mutation (Fig. 2*D*).

In at least two prior reports, thiol modification or oxidomimetic substitution in Hsp70 chaperones has generated increased holdase capacity, binding substrate without ATP-regulated release, and therefore resulting in a dominant negative effect on protein refolding (32, 33). To assess the possibility that a C264/C303 oxidomimetic displays similar dominant negative properties, we titrated 0.2 μM additional Ssa1 or Ssa1-2CD into a pre-existing chaperone cocktail containing 0.1 μM Ssa1 as well as subsequently doubling cochaperone ratios to ensure that competition was not a limiting factor. We found that compared with Ssa1 alone, the Ssa1/Ssa1-2CD pool was hindered in refolding ability (Fig. 2*E*). This suggests that the Ssa1-2CD oxidomimetic may nonproductively bind substrate and inhibit refolding in a dominant negative manner. To assess the potential of Ssa1 dimerization *via* oxidative disulfide bond formation, we subjected Ssa1 to treatment with hydrogen peroxide at similar concentrations used in our experiments, but no altered migration indicative of dimer formation was observed (Fig. S4*B*). We also explored whether reduced interaction with the NEF Sse1 contributed to the deficiency in 2CD activity but determined that even in reactions lacking Sse1, Ssa1-2CD was unable to refold FFL as efficiently as Ssa1 (Fig. S1*C*). Altogether, these results substantiate the negative functional effects of thiol oxidation on protein folding by Ssa1.

Ssa-2CD is incapable of functioning as the sole SSA isoform and is dominant negative

To complement our *in vitro* studies, we addressed consequences of Ssa1 oxidation through the genetic cysteine null and oxidomimetic Ssa1 mutants. We initially attempted to express *ssa1-2CD* as the sole cytosolic *SSA* gene in a quadruple *ssa1Δssa2Δssa3Δssa4Δ* deletion background (43). This strain contained a WT copy of *SSA1* on a *URA3*-selectable plasmid and was in addition transformed with an *HIS3*-selectable plasmid expressing WT *SSA1* or the *ssa1-2CS* or *ssa1-2CD* mutants. A plasmid shuffle technique was used to selectively isolate colonies that possessed only the *HIS3* plasmid *via* plating on 5-fluoroorotic acid media. Surprisingly, all recovered yeast colonies expressing *SSA* alleles grew at identical rates when plated (Fig. S2*A*), inconsistent with the slow-growth phenotype previously reported for the *ssa1-2CD* mutant (27). Sequencing of the recovered *HIS3*-marked plasmid revealed that the *ssa1-2CD* allele had converted to the WT sequence encoding the original cysteine residues (Fig. S2*B*). We hypothesize that this was due to a recombination event between the two plasmids, whereby the likely inability of *ssa1-2CD* to function as the sole expressing cytosolic *SSA* gene resulted in selection for rare allele exchange events (Fig. S2*C*). After several attempts resulting in either no viable colonies or only allele-exchanged colonies, we concluded that the *ssa1-2CD* allele is incapable of sustaining viability as the sole cytosolic *SSA* isoform because of the functional defects demonstrated in Figures 1 and 2.

We elected to continue with oxidomimetic expression *in vivo* in an *ssa1Δ ssa2Δ* deletion background, where Ssa3/4 are present at low levels to support viability, but cell growth is still significantly impaired in nonstressed conditions (27). We in addition wanted to ensure that expression of the WT and mutant alleles best represented natural levels and examined different heterologous promoters for suitability. We found that *SSA1* allele expression from the low-expressing *CYC1* promoter on centromeric (*CEN*) yeast expression vectors resulted in diminished growth for all genotypes, suggesting general Ssa protein insufficiency. However, expression from the stronger CEN-*TEF* vector backbone resulted in normal growth for *SSA1* and *ssa1-2CS* strains, whereas the *ssa1-2CD* and empty vector control both grew at rates similar to each other and consistent with previous reports (Figs. 3, *A* and *B* and S3*A*) (27). Immunoblots confirmed that Ssa1 protein levels were expectedly lower driven from the *CYC1* promoter in *ssa1Δ ssa2Δ* cells as compared with the DS10 parent strain (Fig. S3, *B* and *C*). Intriguingly, *TEF*-driven Ssa1 protein levels were similar between *SSA1*, *ssa1-2CS*, and the parent DS10 strains, but the *ssa1-2CD* allele clearly produced lower levels of Ssa1-2CD protein (Fig. S3, *B* and *C*). We reasoned that Ssa1-2CD

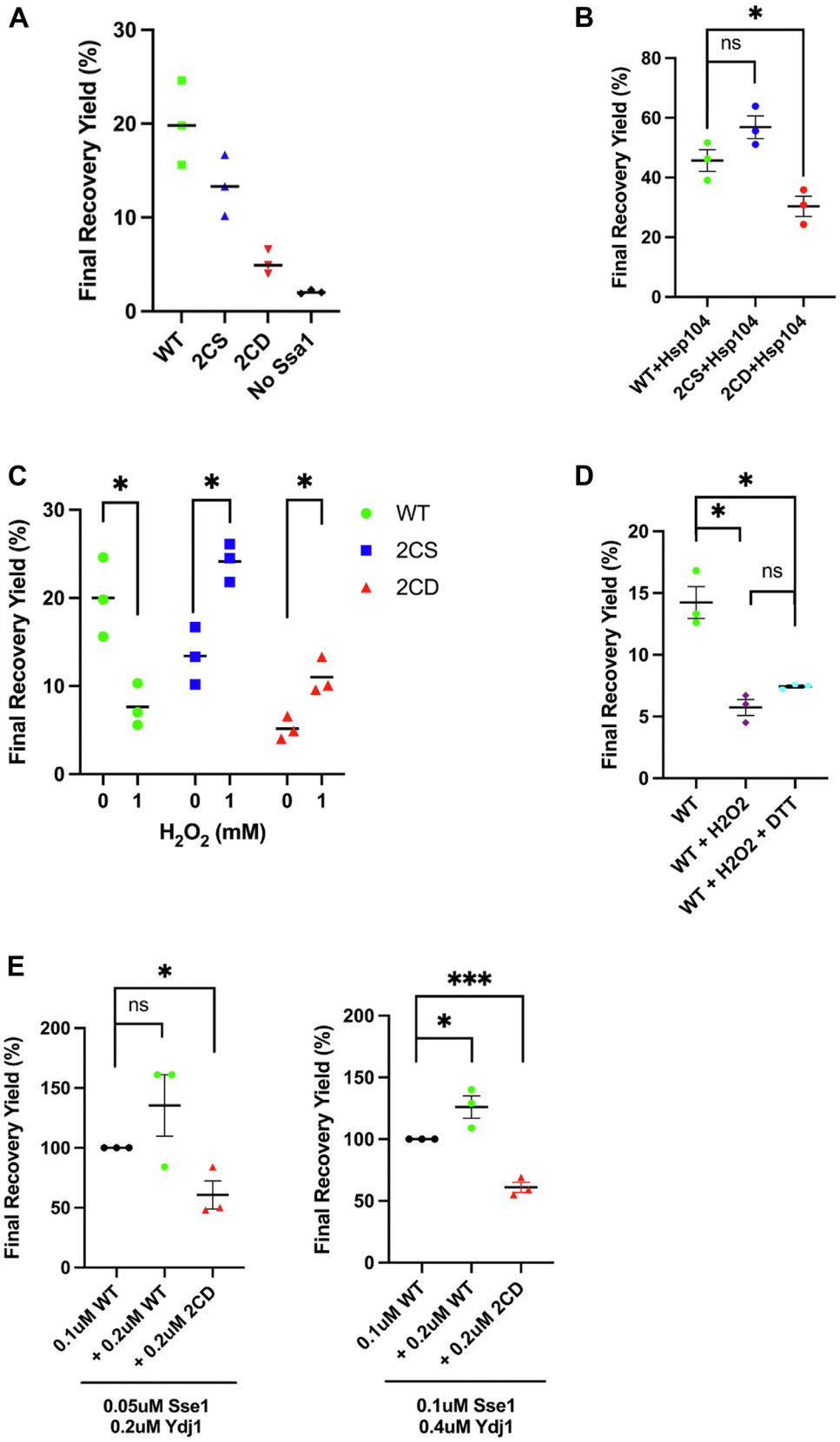

Figure 2. Mimicked and exogenous thiol oxidation negatively impacts *in vitro* protein refolding. *A*, end-point measurements of firefly luciferase (FFL) recovery over 90 min in the presence or the absence of 0.1 μM of the indicated Ssa1 protein and cochaperones Ydj1 (0.2 μM) and Sse1 (0.05 μM), as described in detail in the Experimental procedures section. *B*, end-point measurements of folding reactions including addition of 1 μM Hsp104. *C*, end-point measurements of folding reactions using Ssa1 variants treated or not with 1 mM hydrogen peroxide. *D*, end-point measurements of folding reactions, indicating the respective protein and subsequent addition of exogenous compounds. *E*, end-point measurements of folding reactions, indicating the respective protein additionally added to reactions as in (*A*). *Bolded horizontal bars* indicate mean, and error bars indicate SEM.

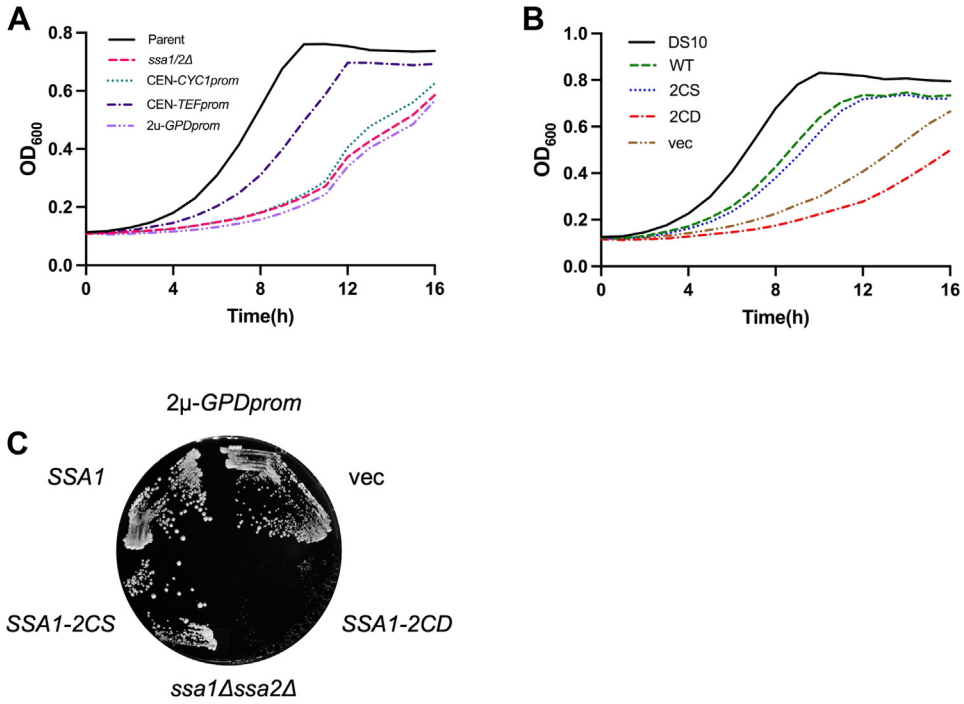

Figure 3. The thiol oxidomimetic *ssa1-2CD* allele displays dominant negative growth impairment. *A*, 16-h growth curve of parent strain DS10, *ssa1Δ ssa2Δ*, and WT *SSA1* driven by the indicated promoter in an *ssa1Δ ssa2Δ* background. *B*, 16-h growth curve of DS10 and indicated *SSA1* allele expression driven by the *TEF* promoter, in an *ssa1Δ ssa2Δ* background. *C*, 48-h plate growth of each indicated *SSA1* allele expressed from the 2μ pRS423TEF vector backbone, in an *ssa1Δssa2Δ* background.

expression was either being actively curtailed or that the mutation resulted in a protein more susceptible to degradation. To test protein stability, we treated cells with the protein translation inhibitor cycloheximide and tracked the existing pool of Ssa1 from each allele by immunoblot, finding that Ssa1-2CD was stable over the course of 3 h (Fig. S3*D*). In addition, Ssa1-2CD did not partition into the insoluble fraction to an extent greater than Ssa1 or Ssa1-2CS (Fig. S4*C*). These results led us to the conclusion that steady-state Ssa1-2CD levels might be restricted in actively growing cells but that the protein itself was not inherently destabilized relative to WT Ssa1.

Our *in vitro* experiments indicated that *ssa1-2CD* exerted dominant negative effects on protein folding. We noted that culture growth rates of the *ssa11-2CD* strain were slower than even the empty vector *ssa1Δ ssa2Δ* control strain, suggesting that expression of the Ssa1-2CD protein at even moderate levels was more detrimental than having no Ssa1 at all (Fig. 3*B*). To further explore this phenomenon, we expressed all *SSA1* alleles from the strong *GPD* promoter on a 2μ vector backbone (44). This level of overexpression of *SSA1* and *ssa1-2CS* reduced growth rates to a level similar to the empty vector background control, consistent with previous reports that chaperone overexpression can be deleterious (Fig. 3*C*) (45). However, overexpression of the *ssa1-2CD* allele resulted in near-total cessation of growth despite the presence of Ssa3/4 in this background, indicating overexpression toxicity beyond the inability to complement loss of Ssa1/2 functions.

Ssa1-2CD fails to physically associate with Hsf1 to repress the HSR

Ssa1 has been recently shown by our laboratory and others to act as a repressor of the HSR transcription factor Hsf1 through physical association with both the amino- and carboxyl-terminal transcriptional activation domains (28, 29, 46). We have also previously published that thiol-modifying compounds induce an HSR in *SSA1*, but not *ssa1-2CS*, cells (27). Consolidating these findings, we hypothesized that thiol stress alters C264 and C303 within Ssa1, inactivating the chaperone resulting in release of Hsf1 and subsequent induction of the HSR. We first confirmed that the HSR was chronically activated in our *ssa1-2CD* strain utilizing an Hsf1-responsive HSE-lacZ reporter (Fig. 4*A*). *ssa1-2CS* cells exhibited appropriate HSR repression, verifying that the endogenous cysteines are not required for Ssa1 to function as a repressor of Hsf1. To test our hypothesis that Ssa1-2CD is defective in Hsf1 association, Hsf1-GFP-FLAG was coexpressed in cells containing either *CYC1*-driven *SSA1* and *ssa1-2CS* or *TEF*-driven *ssa1-2CD* alleles to control for differential Ssa1 protein levels, and coimmunoprecipitations were performed. Both Ssa1 and Ssa1-2CS associated with Hsf1, but no detectable signal was observed for Ssa1-2CD (Fig. 4, *B* and *C*). None of the Ssa1 proteins were found to associate with the GFP-FLAG control, confirming specificity of Hsf1 binding. These data indicate that the oxidomimetic Ssa1-2CD is unable to productively bind the bipartite contact sites on Hsf1 and provide a molecular mechanism to explain oxidative stress sensing by Hsf1 *via* Cys264/303 of Ssa1.

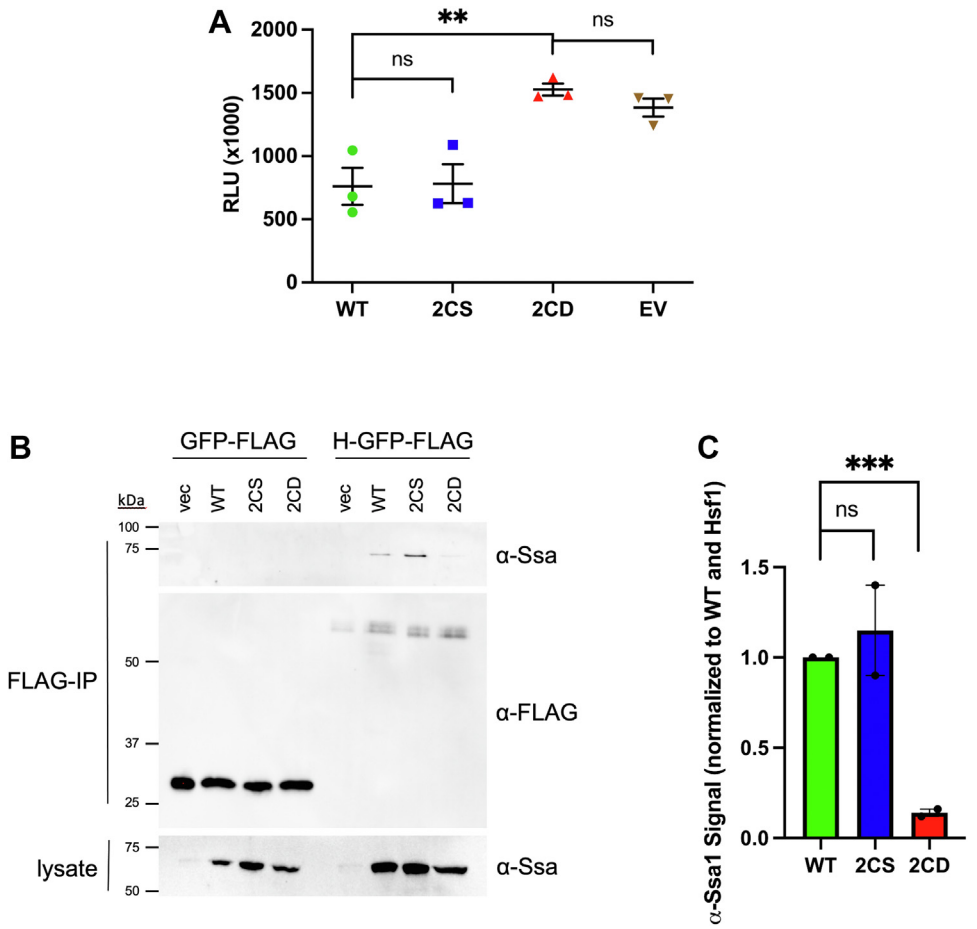

Figure 4. Ssa1-2CD fails to bind and repress the heat shock regulator Hsf1. *A*, HSE-lacZ activity of strains containing WT and mutant *SSA1* alleles grown at 30 °C. To normalize Ssa1 protein levels, *SSA1* and *ssa1-2CS* were expressed from the CYC1 promoter and *ssa1-2CD* from the stronger TEF promoter. *B*, coimmunoprecipitation of tagged Hsf1-GFP-FLAG or GFP-FLAG control and the indicated Ssa1 proteins. *C*, quantification of assay detailed in (*B*), normalized for load and measured as the ratio of signal compared with WT. *Bolded horizontal bars* indicate mean, and error bars indicate SEM.

ssa1-2CD is defective in protein folding, solubilization, and refolding in vivo

Hsp70 proteins are critical factors for ensuring proteostasis (5). We hypothesized that mimicked cysteine oxidation would have negative consequences for Hsp70 protein surveillance activities. Data presented in Figure 2 demonstrate that the Ssa1-2CD protein or exogenously oxidized Ssa1 are defective in protein folding. To complement the *in vitro* folding assays, we coexpressed with the *SSA1* alleles as previously generated and well-documented FFL-GFP fusion protein known to require the Hsp70 chaperone system for folding in living cells (47, 48). To monitor *de novo* folding of nascent polypeptides, we utilized the methionine-repressible promoter of the FFL-GFP plasmid to induce expression of FFL in log phase cells. FFL activity was measured by luciferase assay over the course of 90 min. The *ssa1-2CS* mutant was able to fully complement the *de novo* folding defect observed in *ssa1Δ ssa2Δ* cells relative to cells expressing *SSA1*, whereas the *ssa1-2CD* mutant was significantly defective (~60% of WT luciferase activity) (Fig. 5*A*). To account for the lower abundance of Ssa1-2CD, we also examined *de novo* folding activity in a *CYC1-SSA1* strain and found that this reduced level of expression still maintained higher FFL activity than observed in the *TEF-ssa1-2CD* background, indicating that absolute protein levels do not explain the reduced capacity for FFL folding seen with Ssa1-2CD (Fig. S3*E*).

Misfolded proteins are known to aggregate in concert with protein chaperones, including sequestrases and disaggregases, and can be visualized *in vivo* using fluorescent tagging approaches (49, 50). To examine the status of properly folded and potentially misfolded FFL, overnight cultures of *SSA1*, *ssa1-2CS*, and *ssa1-2CD* and a vector control containing the FFL-GFP–expressing plasmid were visualized using fluorescence microscopy. Micrographs displaying representative images show that FFL-GFP was found to be fully soluble in *SSA1* and *ssa1-2CS* strains, whereas *ssa1-2CD* and the vector control exhibited large foci, visible as fluorescent puncta that were present in a significantly higher percentage of cells (Fig. 5, *B* and *C*). As an additional orthogonal approach to complement our *in vitro* findings, we determined the ability of each strain to refold heat-denatured substrate. Log-phase cells were washed to remove methionine and induce FFL-GFP expression to generate a pool of substrate. Cycloheximide was then added to prevent additional FFL-GFP expression, and steady-state luminescence activity was measured. Cellular FFL-GFP was denatured by incubating cultures at 42 °C, followed by a

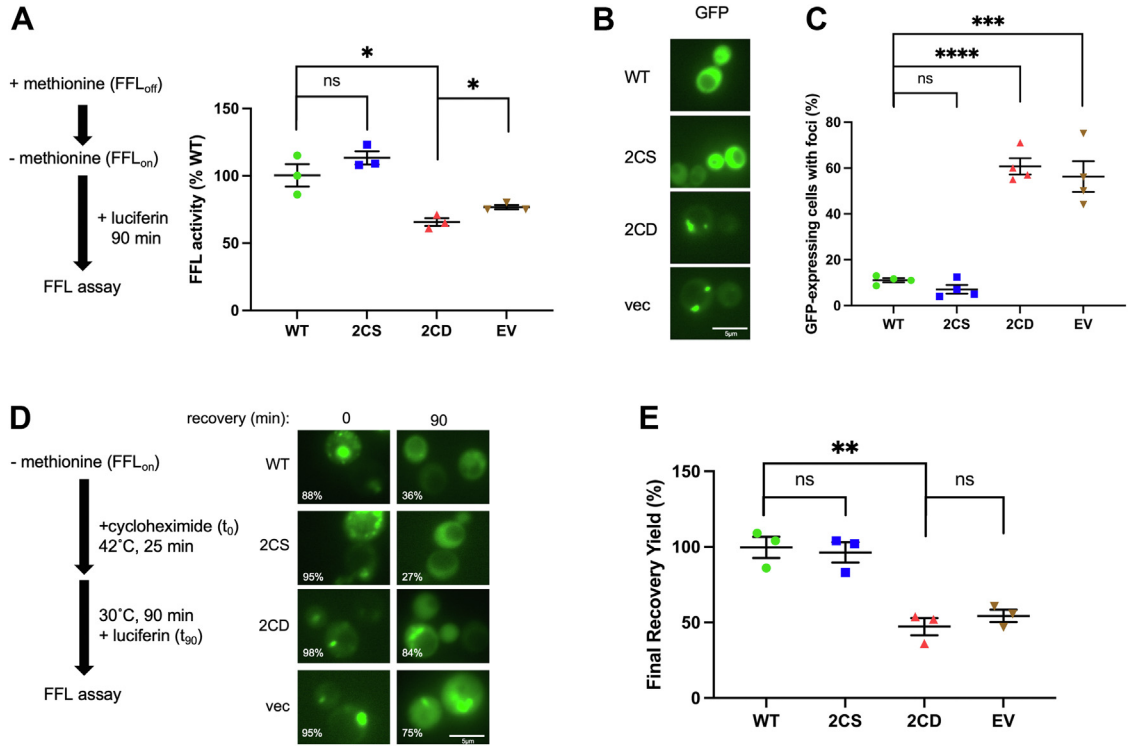

Figure 5. The *ssa1-2CD* mutant exhibits multiple deficiencies in proteostasis. *A*, end-point *de novo* folding ability of *SSA1* or mutant *ssa1* alleles as measured by luciferase activity assay, monitored over 90 min. *B*, images representing firefly luciferase (FFL)-GFP fluorescence in *SSA1* or *ssa1* mutant strains grown overnight at 30 °C. *C*, quantification of (*B*) in terms of foci per cell. Each data point represents percentage of cells containing foci from a minimum of 50 cells per replicate. *D*, schematic of FFL-GFP recovery assay and representative micrographs detailing *SSA1* and mutant *SSA1* strains at 0 and 90 min after initiation of cycloheximide chase. Number of cells containing foci are shown as an *inset* percentage. *E*, quantification of assay detailed in (*D*), measured as the percentage of FFL-GFP chemiluminescence activity at t_{90} in *SSA1* and respective ssa1 mutant strains, relative to the same sample at t_0. *Bolded horizontal bars* indicate mean, and error bars indicate SEM.

recovery period at 30 °C. Cells were then visualized by fluorescence microscopy, and luminescence was determined. All strains contained puncta immediately after heat shock, and while *SSA1* and *ssa1-2CS* strains resolved FFL-GFP aggregates, *ssa1-2CD* and the empty vector control failed to do so (Fig. 5*D*). These results were mirrored when FFL enzymatic activity was examined, with the *ssa1-2CD* and the empty vector control only managing to restore approximately 50% of original preheat shock FFL-GFP activity (Fig. 5*E*). Taken together, these data indicate that the mimicking of chronic oxidation of Ssa1 cysteines 264 and 303 dramatically undermines general proteostasis, with negative consequences for the proper folding of nascent translating polypeptides and the refolding of stress-denatured proteins.

ssa1-2CD cells fail to clear permanently misfolded proteins from aggregates

Chaperones, most notably the Hsp70 system, are tightly integrated into the protein quality control system and selectively regulate protein degradation *via* presentation of substrate to ubiquitin ligases (51). To investigate how thiol modification of Ssa1 cysteines affects degradation of misfolded proteins, we utilized a well-characterized substrate, tGnd-GFP (51, 52). This artificial construct contains a truncated version of the Gnd1 protein fused to GFP that results in an unfoldable substrate with defined kinetics of degradation through the ubiquitin–proteasome pathway. We first expressed tGnd-GFP in the presence of the *SSA1* alleles and observed a greater than twofold increase in steady-state levels of the substrate by immunoblot in the *ssa1-2CD* and vector control strains (Fig. 6, *A* and *B*). To determine the status of accumulated tGnd-GFP, log phase cells were treated with cycloheximide to stop further synthesis and imaged by fluorescence microscopy. Representative micrographs show the presence of tGnd1-GFP foci presence in all strains at t_0, indicating that misfolded protein was sequestered into protein aggregates (Fig. 6*C*). After 90 min, foci remained in a significantly higher amount of *ssa1-2CD* and vector control cells compared with *SSA1* and *ssa1-2CS* cells, where foci were largely eliminated, indicative of impaired substrate processing and degradation (Fig. 6, *C* and *D*). Taken together, these data support the conclusion that Ssa1 cysteine oxidation, as mimicked by aspartate substitution, renders the chaperone defective in promoting the degradation of terminally misfolded substrates.

Discussion

In this study, we explored in detail the functional consequences of oxidation of two key cysteines in Ssa1 previously demonstrated to be required for activation of the HSR by thiol-reactive molecules *via* genetic and chemical approaches. Analysis using purified proteins revealed that Ssa1-2CD, but not the Ssa1-2CS mutant, is compromised for ATP binding

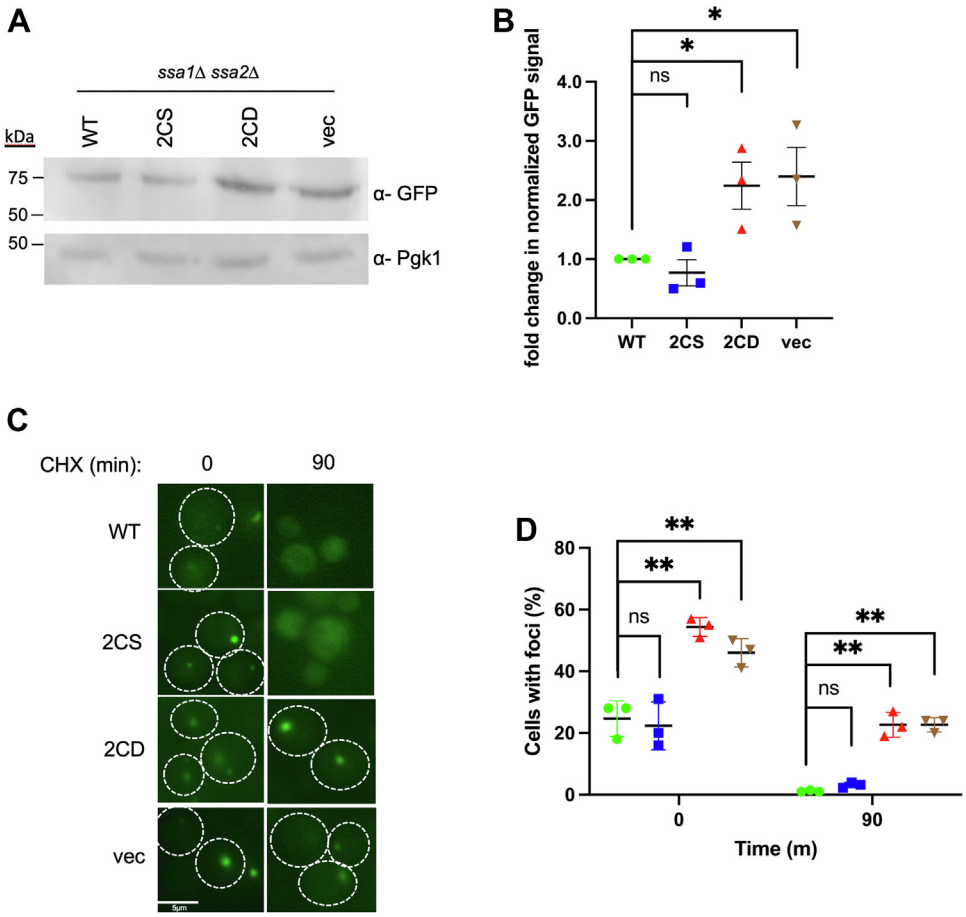

Figure 6. Degradation of the misfolded protein tGND-GFP is chronically impaired in *ssa1-2CD* cells. *A*, Western blot analysis of steady-state levels of the chronically misfolded protein tGND, coexpressed with *SSA1* or mutant *ssa1* alleles taken from cells in log phase. *B*, quantification of signal in *A*, measured as fold change of each mutant allele relative to *SSA1*, from three replicate blots. *C*, representative images of cycloheximide chase, monitoring tGND-GFP foci presence over 90 min for each respective allele. *D*, quantification of images in *C*, with each data point representing a percentage of cells containing foci from a minimum of 50 cells per replicate. *Bolded horizontal bars* indicate mean, and error bars indicate SEM.

and hydrolysis, as well as ATP-dependent protein folding. Nearly identical results were observed upon treatment of WT Ssa1 protein with hydrogen peroxide, validating the utility of the aspartic acid substitution to mimic the sulfinic acid state of the cysteine thiol group after oxidation. Importantly, the nonreactive cysteine null substitution to serine (Ssa1-2CS) was impervious to hydrogen peroxide at concentrations that impaired Ssa1 enzymatic activity *in vitro*. We can therefore conclude that cysteines 264 and 303 are exclusively responsible for the observed behaviors *in vitro* and *in vivo*, at least under our experimental conditions. In addition to these two cysteines in Ssa1 located on lobe IIB within the NBD, a third cysteine residue is conserved in most Hsp70 homologs deeper within the nucleotide-binding cleft (C15 in Ssa1). Our results suggest that C15 is not a critical target for oxidation for Ssa1. This finding contrasts with previous work from the Sevier laboratory where C63 of the endoplasmic reticulum–resident Hsp70 Kar2/BiP was found to be sensitive to oxidation (53). However, both yeast Kar2 and mammalian BiP lack homologous cysteines 264 and 303, complicating a direct comparison. Notably, all three cysteines are sensitive to modification by the strong alkylating agent NEM; NEM-Ssa1 also exhibited the same range of functional defects as our oxidomimetic mutant and peroxide-treated Ssa1 (33). NEM-treated Ssa1 displayed altered trypsinization profiles and intrinsic tryptophan fluorescence indicative of structural deformation within the NBD (34). In human Hsc70, it was found that modification of nucleotide pocket–facing C17 displaced a catalytic magnesium ion that is crucial for nucleotide hydrolysis by increasing the distance of that magnesium from several interacting residues (54). These results are also consistent with previous data that methylene blue oxidizes cysteines 267 and 306 in the stress-inducible human Hsp70, resulting in reduced ATP binding and hydrolysis (30). *In silico* modeling in this report suggested that oxidation occurs stepwise, where C306, located on the outer surface of lobe IIB of the NBD, is oxidized first, resulting in a conformational change that displaces the inner lobe cysteine, C267, into a solvent-exposed cleft. This structural deformation may increase the accessibility or reactivity of the thiolate anion of cysteine 267 and ultimately disfigure the entire NBD to reduce nucleotide-binding affinity and dependent enzymatic activities. This model is in complete agreement with a previous study of ours demonstrating that reaction of C264 in Ssa1 with a 4-hydroxynonenal alkyne and subsequent derivatization *via* click chemistry was lost in a C303S mutant (27).

We found that addition of Ssa1-2CD inhibited productive FFL refolding by Ssa1. This result is consistent with previous data that NEM-Ssa1 likewise blocked Ssa1-dependent folding but not the ability to inhibit aggregation of misfolded protein. Indeed, oxidation, alkylation, or substitution with a bulky side-chain residue of C63 in Kar2 significantly enhances the "holdase" ability of that Hsp70 (53). These findings are all consistent with a model wherein oxidation disrupts productive allosteric communication between the NBD and SBD but does not affect and may even enhance polypeptide binding by the SBD, resulting in competition for Hsp70-binding sites and restricting productive folding reactions. Such a model would explain the semidominant negative growth phenotypes we observed upon expression of *ssa1-2CD* in cells that still retained expression of the inducible *SSA* isoforms Ssa3 and Ssa4. Importantly, this model also provides a mechanism by which oxidation of only a portion of the highly abundant pool of Ssa1 and Ssa2 could exert deleterious effects on cell functions and growth, as it is highly unlikely that transient exposure to oxidants would modify the majority of available Hsp70. Unlike the findings of Wang *et al.* (53), wherein oxidized Kar2 renders cells hyper-resistant to oxidative stress, we found no evidence for any gain-of-function phenotypes in the *ssa1-2CD* strain. However, it is important to note that our Ssa1-2CD mutation mimics the difficult-to-reverse sulfinic acid thiol state, and reversibility has been demonstrated to be a key factor for oxidative regulation, as extensive oxidative stress inactivates ATP-dependent chaperones (15, 55).

As demonstrated by substitution with serine or alanine residues, cysteines 264 and 303 in Ssa1 are dispensable for growth at elevated temperatures, as is C63 in Kar2/BiP (53). However, the cysteines are essential for activation of stress responses and cytoprotection by cells exposed to oxidizing compounds (27, 53). This pattern is indicative of a residue that has been evolutionarily conserved to sense and react to an oxidative stressor. The reversibility of cysteine modification is especially useful as a signal, as it allows for chaperones that contain them to switch between conformations that may have different purposes, with the additional involvement of redox management systems such as the thioredoxin and glutathione pathways (56). A key example of the utility of Ssa1 cysteine signaling is the transient activation of the HSR upon treatment with alkylating agents or oxidizing agents. Because yeast Hsf1 lacks cysteines, it is unable to directly respond to such insults in contrast to human HSF1 that is directly modified on exposed cysteines to activate the HSR to rebalance proteostasis (57). C264/C303 of Ssa1 therefore play an elegantly analogous role of oxidative sensor in yeast *via* the recently described direct repression of Hsf1 by the chaperone. We now for the first time connect these two concepts by showing that Ssa1-2CD fails to bind either known site on Hsf1 *in vivo*, resulting in a chronically elevated HSR. Interestingly, Ssa3/4 do not contain the cysteine found in the outer face of lobe IIB, C303, only the pocket-facing cysteine C264. Following the *in silico* model, this makes Ssa3/4 less vulnerable to oxidation, which we believe is advantageous in a stressed environment. Ssa3/4 are expressed at much lower levels relative to Ssa1/2 but are upregulated under stress exposure (7). Interestingly, after aligning several Hsp70 proteins found in yeast, Ssc1 was found to lack all three critical cysteine residues, which our model suggests may render it resistant to cysteine-based oxidative regulation (Fig. S5). Correspondingly, the nucleotide exchange factor Mge1 appears to be a functional sensor for mitochondrial oxidative stress (58–60). Returning to the context of HSR regulation, one can therefore envision a scenario wherein upon oxidative stress, Ssa1 is inactivated, Hsf1 is liberated, and a potent HSR ensues resulting in upregulation of Ssa3/4. These inducible chaperones can then bind to the same sites on Hsf1 to attenuate the HSR and have the added benefit of resisting further oxidative damage/signaling.

We found that multiple aspects of Ssa1 function are compromised in the *ssa1-2CD* strain. Because it would be impossible to deconvolute the pleiotropic effects of whole-cell treatment with exogenous oxidants, a genetic approach using the oxidomimetic substitution is the best approach to understanding functional consequences of Hsp70 modification. We uncovered profound deficiencies in *de novo* protein folding, extraction of misfolded proteins from aggregates, and clearance of terminally misfolded proteins—all salient aspects of proteostasis. Together, these phenotypes likely account for the severe slow growth phenotype of the *ssa1-2CD* mutant, its inability to serve as the sole *SSA* isoform, and the observed high rate of gene reversion when we attempted the plasmid shuffle approach. Our findings are consistent with and significantly extend previous findings that an oxidomimetic allele of Hsp72 failed to support tau stabilization in human HeLaC3 cells (30). Notably, induction of Ssa3/4 *via* derepression of the HSR is insufficient to restore proteostasis in the *ssa1-2CD* strain but is required to allow viability. It is therefore possible that the *ssa1-2CD* mutant may be entirely dysfunctional in supporting folding and regulated degradation of the proteome but that a reduced level of proteostasis is maintained by Ssa3/4.

Further work is required to fully understand the consequences of oxidative stress on cell and tissue proteostasis as it relates to human health. Many industrial pollutants are oxidants or thiol-reactive molecules (*e.g.*, heavy metals, acroleins) (61). Cigarette smoke contains a wide range of thiol-reactive compounds that are known to deplete cellular glutathione levels (62). Accumulation of oxidative damage is widely considered to be a key driver of aging, potentially linked to endogenous ROS generated *via* mitochondrial dysfunction. Indeed, oxidation of a methionine residue in the mitochondrial Mge1 protein, a cofactor of mitochondrial matrix Hsp70, inhibits protein translocation into the organelle resulting in oxidant hypersensitivity (58). Clearly more attention must be paid to the impacts of oxidative stress on the protein quality control network going forward.

Experimental procedures

Strains, plasmids, and yeast cultivation

Yeast strains were derived from either DS10 (*MATa ura3-52 lys1 lys2 trp1-1 his3-11,15 leu2-3112*) or BY4741 (*MATa, his3Δ1; leu2Δ0; met15Δ0; ura3Δ0*) parent strains. The

ssa1Δssa2Δ strain (*SL314, MATa ura3-52 lys1 lys2 trp1-1 his3-11,15 leu2-3112 ssa1::HIS3, ssa2::LEU2*) was generously provided by the Craig laboratory and is isogenic with DS10 (8). Complementation of the lethal *ssa1Δssa2Δ ssa3Δssa4Δ* strain was conducted using a standard yeast plasmid shuffle technique, with a *URA3*-based *SSA1*-expressing plasmid (a kind gift from the Truman laboratory). The *SSA1* allele plasmids (p413TEF, p413CYC, and p423GPD) were constructed by PCR mutagenesis and amplification of the SSA1 ORF using standard cloning methodology with 5′ SpeI and 3′ XhoI restriction sites. All mutants were confirmed using DNA sequencing. All plasmids were transformed into yeast using the rapid yeast transformation protocol (63). The FLAG-tagged Hsf1-expressing plasmid was used as previously published (28). The pTHD3HA-tGND-GFP plasmid was a kind gift from Dr Randolph Hampton, University of California, San Diego. The HSE-lacZ plasmid was reported previously (64). The p425MET25-FFL-GFP-leu2::URA3 plasmid was used as previously described (47). The 6XHis-Smt3-SSA1 plasmid was kindly provided by Dr Nadinath Nillegoda (Monash University, Australia). *S. cerevisiae* strains were cultured in yeast extract, peptone, dextrose medium or synthetic complete (SC) medium (Sunrise Science). For growth curve analysis, cells were grown overnight at 30 °C. Cells were then subcultured and grown to midlog phase (absorbance at 600 nm = 0.6–0.8) and then diluted to absorbance at 600 nm = 0.1 in fresh media. Growth was monitored using a Synergy MX (BioTek) microplate reader for 16 h with shaking at 30 °C. Petri plate growth analysis was for 2 days at 30 °C. Cells containing the HSE-*lacZ* reporter were grown to log phase and diluted to an absorbance of 0.8 at 600 nm. About 50 μl of Beta-Glo reagent (Promega) and 100 μl of liquid culture was added to each well in a 96-well microplate and measured for beta galactosidase activity using the Synergy MX microplate reader.

Protein purification

Proteins were isolated as previously described, with several alterations (35). Briefly, *SSA1* coding regions were amplified from p413TEF plasmids and subcloned into the pSUMO vector with a 6XHis-Smt3 tag (gifted from the Nillegoda laboratory) (35, 65). Plasmids were transformed into BL21(DE3) *Escherichia coli* in addition containing the pRARE plasmid and grown overnight in LB ampicillin/kanamycin at 37 °C. Subcultures were then grown to log phase (absorbance at 600 nm = 0.6), and expression was induced with 0.5 mM IPTG (MilliporeSigma) for 3 h at 30 °C, then cells were collected by centrifugation, washed, and flash frozen for storage at −80 °C. The following day, cells were lysed in 30 ml buffer K (50 mM Hepes–KOH, pH 7.5, 750 mM KCl, and 5 mM $MgCl_2$) with DNAse, RNAse, protease inhibitors (PIs), and 1 mM PMSF. Suspensions were sonicated on ice to lyse, and cell debris was removed by centrifugation for 10 min at 12,500 RCF at 4 °C. Supernatant was removed, and the suspension was again centrifuged. The supernatant was brought up to 30 ml with buffer K and nutated for 1 h at 4 °C with 1 ml bed volume of buffer K-equilibrated His-Pur cobalt resin (Thermo Fisher Scientific), adding 30 μl fresh PI, 1 mM PMSF, and 50 μl of 100 mM ATP (pH 7.5). The suspension was centrifuged at 4 °C for 10 min at 9000 RCF, and supernatant was removed. The resin was washed twice with 30 ml of buffer KC (50 mM Hepes–KOH, pH 7.5, 750 mM KCl, 5 mM $MgCl_2$, and 30 mM imidazole) plus fresh PI and PMSF. Washes consisted of resuspension and hand nutation for 30 s, 3 min on ice, a 2 min spin at 5500 RCF in chilled rotors, 3 additional min on ice, followed by supernatant removal. Final supernatant was removed, and the resin was incubated three times with 500 μl of buffer KE (50 mM Hepes-KOH, pH 7.5, 750 mM KCl, 5 mM $MgCl_2$, and 300 mM imidazole), centrifuged for 30 s at 6000 RCF, and supernatant was passed through a filter column to elute proteins. All elutions were then concentrated by Vivaspin column (Cytiva) and placed into dialysis tubing, then incubated overnight with stirring in 1 l of chilled buffer KL (50 mM Hepes–KOH, pH 7.5, 30 mM KCl, and 5 mM $MgCl_2$) to remove imidazole. The SUMO protease Ulp1 (lab isolated) was added to the dialyzed protein sample and incubated at room temperature for 1 h. About 500 μl of buffer KL–equilibrated resin was added, and the mixture was nutated at 4 °C for 1 h. A filter column was used to separate beads from cleaved protein isolate. About 10% glycerol was added, and proteins were either frozen at −80 °C or immediately further purified using an AKTA pure ion exchange chromatography system (Cytiva) and HiTrap Q HP columns (Cytiva), testing fraction activity by quantifying ATP hydrolysis. Proteins were again concentrated with 10% glycerol, separated into aliquots, and snap frozen at −80 °C. Isolated Ydj1 was a generous gift from Elizabeth Craig, and Sse1 was from a previously isolated laboratory stock (66). Purified Hsp104 protein was a kind gift of the Tsai laboratory (Baylor College of Medicine).

ATP-binding assay

For each respective protein sample, 25 μl of ATP-agarose bead volume was washed three times with 1 ml chaperone buffer (50 mM Hepes–KOH, pH 7.5, 50 mM KCl, 5 mM $MgCl_2$, and 5 mM DTT) in a siliconized tube. Beads were resuspended in 500 μl chaperone buffer with 1 μM final concentration of protein isolate. Suspensions were nutated at 4 °C for 30 min and washed five times with 1 ml chaperone buffer + 1.5% Triton X-100 (30 s spin at 6000 RCF, on ice in between). After removing supernatant, beads were transferred to a new siliconized tube to negate tube-bound protein, and 50 μl of chaperone buffer plus 50 μl of 2× SDS-PAGE sample buffer were added, followed by incubating at 65 °C for 20 min prior to gel loading to elute proteins.

ATPase assay

ATP hydrolysis was determined using a malachite green–based assay (MilliporeSigma) to measure phosphate release. Purified Ssa1 was diluted to 0.1 μM, with or without 0.2 μM Ydj1, in 20 μl total volume of reaction buffer in a 96-well plate. About 10 μl of 4 mM ATP was added to each well, and the plate was incubated with a cover for 90 min at 30 °C, followed by the addition of 150 μl of the malachite green reagent. The

colorimetric reaction proceeded for 30 min at room temperature before measuring absorbance. Absorbance values were read and converted to picomoles of phosphate using a standardized phosphate curve. Values are reported as specific activity (pmol ATP/μg Hsp70/min).

In vitro *FFL recovery assay*

Refolding of denatured FFL was assessed as reported previously, with slight alteration (33). In short, 200 μM FFL protein was incubated 1:1 with denaturing buffer (50 mM Hepes–KOH, pH 7.5, 50 mM KCl, 5 mM $MgCl_2$, 5 mM DTT, and 3 M guanidinium HCl) at room temperature for 30 min to denature. Denatured FFL (1 μM) was added to a chaperone mixture containing the respective Ssa1 (0.1 μM), Ydj1 (0.2 μM), Sse1 (0.05 μM), 5 mM ATP, and Hsp104 when applicable (0.1 μM) and then brought to a final reaction volume of 100 μl with chaperone buffer. About 5 μl of reaction mixture was diluted into a well containing 200 μl of chaperone buffer prior to measurement. To measure activity of properly folded luciferase, 20 μl of luciferin (222 μM) was added to 10 ml of chaperone buffer, and 10 μl was autoinjected into each well and chemiluminescence signal measured. Activity was determined at indicated time points, and raw numbers were converted to a percentage through comparison to activity of a nondenatured control in the same volume.

Treatment of chaperones with hydrogen peroxide

A hydrogen peroxide oxidation regimen was amended from a previously described protocol (30). Ssa1 proteins (5 μM) were incubated with 1 mM hydrogen peroxide for 1 h at 37 °C, followed by 50-fold dilution to final assay concentration. For subsequent reduction, WT was incubated with 20 mM DTT after hydrogen peroxide treatment, and the mixture allowed to incubate at room temperature for 10 min, as previously described (34).

Trypsin digestion

Chaperones were subjected to trypsin digestion as previously described (37). In short, 1.5 μg of Ssa1 was incubated with 1 mM of the respective nucleotide for 10 min at room temperature. Trypsin (1 mg/ml) was then added and reactions incubated for 20 min at room temperature, before stopping the reaction by adding 6× SDS-PAGE sample buffer.

Preparation of cell extracts and immunoblotting

Cells were grown overnight, subcultured, and grown to midlog phase (absorbance at 600 nm = 0.6–0.8). Proteins were extracted by glass bead lysis as previously described (67). Proteins were analyzed by separation on SDS-PAGE gels (8–12%) and transferred to polyvinylidene difluoride membrane (EMD Millipore). Immunoblots were imaged using an anti-Ssa1/2 polyclonal antibody at a 1:10,000 dilution, anti-FLAG monoclonal antibody at a 1:4000 dilution (MilliporeSigma), or anti-GFP at a 1:5000 dilution (Roche) using a previously described procedure (67). Blots were sprayed with WesternBright ECL Spray (Advansta) and imaged using the ChemiDoc MP Imaging System (Bio-Rad). Bands were quantified using Image Studio Lite (LI-COR Biosciences). To monitor chaperone stability, 100 μg/ml cycloheximide was added to log phase cultures.

Hsf1 immunoprecipitation

Immunoprecipitation was performed as previously described (28). In short, 30 ml of cells was lysed by glass beads, and total lysate was coincubated with anti-FLAG M2 Affinity gel (MilliporeSigma) in a total volume of 700 μl of TEGN buffer (20 mM Tris–HCl, pH 7.9, 0.5 mM EDTA, 10% glycerol, 50 mM NaCl), plus PIs, nutating for 2 h at 4 °C. Beads were washed eight times using 750 μl of TEGN + PI, followed by elution of proteins using 40 μl of FLAG peptide (200 μg/ml) at room temperature for 25 min 6× SDS-PAGE sample buffer (350 mM Tris–HCl, pH 6.8, 36% glycerol, 10% SDS, 5% beta-mercaptoethanol, and 0.012% bromophenol blue) was added to samples and incubated at 65 °C for 20 min to elute.

Fluorescence microscopy

For all experiments, yeast live cells were imaged as described previously (68). In short, cells were wet-mounted on slides and imaged using the 100× objective of an Olympus IX81 microscope, using an FITC filter to visualize GFP. For each experiment, identical exposure times were used. For foci counts, strains were grown overnight in SC-HIS-URA, and late growth stage cells were imaged.

In vivo *FFL assays*

FFL-GFP *de novo* assays were carried out as previously specified (47). Briefly, indicated strains containing the 413TEF *SSA1*-expressing plasmid and p425MET25-FFL-GFP-leu2::URA3 were grown overnight in SC-URA-HIS at 30 °C. About 100 μl of additional methionine was added to repress plasmid expression. Cells were subcultured in fresh media to log phase absorbance at 600 nm = 0.8, 5 ml of cells were harvested by centrifugation, and washed to remove all methionine. Cells were resuspended in 5 ml of SC-URA-MET to induce FFL-GFP expression, and activity was measured at the indicated time points by adding 10 μl of 222 nM luciferin in a microplate reader.

Refolding assays were performed similarly to *de novo* FFL activity assays, but after 1 h of induction, 100 mg/ml of cycloheximide was added to stop protein synthesis. Cells were then subjected to heat denaturing at 42 °C for 15 min, then incubated at 30 °C for recovery. FFL-GFP activity was measured by adding 10 μl of 222 nM luciferin in a microplate reader or imaged for foci.

tGND-GFP protein turnover

Steady-state levels of the terminally misfolded protein tGND were performed essentially as described (51). In brief, BY4741 *ssa1Δssa2Δ* cells containing the pTHD3HA-tGND-GFP plasmid and relevant p413TEF *SSA1* allele plasmid were grown to early log phase in SC-HIS-URA (absorbance at 600 nm = 0.5). About 1 ml of cells were collected, washed,

resuspended in 177 μl of 1.85 M NaOH, and left on ice for 10 min. About 177 μl of cold 55% trichloroacetic acid was added, and the sample incubated on ice for an additional 10 min. Cells were centrifuged in a cold room at 7200 RCF for 1 min, and supernatant was removed. The pellet was resuspended in 500 μl of ice-cold acetone and centrifuged. The supernatant was removed, and 100 μl per absorbance of 2× urea buffer (1% SDS, 8 M urea, 10 mM Mops, 10 mM EDTA, pH 6.8, 0.01% bromophenol blue, and 1 mM PMSF) was added. Suspensions were sonicated for 5 min, and samples were placed at 65 °C for 20 min, followed by an additional 5 min of sonication. Cells were again centrifuged, and supernatant was moved to a new tube and frozen prior to SDS-PAGE separation and immunoblot. For microscopy, cells were grown to early log phase (absorbance at 600 nm = 0.5) in SC-HIS-URA, and 100 μg/ml cycloheximide was added to cultures. Cells were imaged for foci at relevant time points.

Statistical analysis

Student's *t* test was used to analyze mean differences between conditions. Prism 9 (GraphPad Software, Inc) was used to analyze averages of end-point measurements of each time point and calculate standard error of the mean. For all significant tests, $^{*}p = 0.05$; $^{**}p = 0.005$; $^{***}p = 0.0005$; and $^{****}p = 0.00005$.

Data availability

All relevant data described are contained within the article and Supporting Information.

Supporting information—This article contains supporting information.

Acknowledgments—We thank Drs Qinglian Liu (Virginia Commonwealth University), Randy Hampton (UC San Diego), Nadinath Nillegoda (Monash University), Elizabeth Craig (University of Wisconsin), Andrew Truman (University of North Carolina, Charlotte), and Francis Tsai (Baylor College of Medicine) for advice and reagents. We in addition thank Santosh Kumar and Anna Konovalova (McGovern Medical School) for protein purification assistance. This study was supported by the National Institutes of Health grant R01GM127287. The content is solely the responsibility of the authors and does not necessarily represent the official views of the National Institutes of Health.

Author contributions—A. S. and K. A. M. conceptualization; A. S. and K. A. M. methodology; A. S. investigation; A. S. writing–original draft; A. S. and K. A. M. writing–review & editing; A. S. and K. A. M. visualization.

Conflict of interest—The authors declare that they have no conflicts of interest with the contents of this article.

Abbreviations—The abbreviations used are: BiP, binding immunoglobulin protein; FFL, firefly luciferase; Hsp70, heat shock protein 70; HSR, heat shock response; NBD, nucleotide-binding domain; NEM, *N*-ethylmaleimide; PI, protease inhibitor; ROS, reactive oxygen species; SBD, substrate-binding domain; SC, synthetic complete.

References

1. Hipp, M. S., Kasturi, P., and Hartl, F. U. (2019) The proteostasis network and its decline in ageing. *Nat. Rev. Mol. Cell Biol.* **20**, 421–435
2. Soto, C., and Pritzkow, S. (2018) Protein misfolding, aggregation, and conformational strains in neurodegenerative diseases. *Nat. Neurosci.* **21**, 1332–1340
3. Peng, C., Trojanowski, J. Q., and Lee, V. M. Y. (2020) Protein transmission in neurodegenerative disease. *Nat. Rev. Neurol.* **16**, 199–212
4. Rosenzweig, R., Nillegoda, N. B., Mayer, M. P., and Bukau, B. (2019) The Hsp70 chaperone network. *Nat. Rev. Mol. Cell Biol.* **20**, 665–680
5. Hartl, F. U., Bracher, A., and Hayer-Hartl, M. (2011) Molecular chaperones in protein folding and proteostasis. *Nature* **475**, 324–332
6. Kityk, R., Kopp, J., and Mayer, M. P. (2018) Molecular mechanism of J-domain-triggered ATP hydrolysis by Hsp70 chaperones. *Mol. Cell* **69**, 227–237.e4
7. Lotz, S. K., Knighton, L. E., Nitika Jones, G. W., and Truman, A. W. (2019) Not quite the SSAme: unique roles for the yeast cytosolic Hsp70s. *Curr. Genet.* **65**, 1127–1134
8. Craig, E. A., and Jacobsen, K. (1984) Mutations of the heat inducible 70 kilodalton genes of yeast confer temperature sensitive growth. *Cell* **38**, 841–849
9. Werner-Washburne, M., Stone, D. E., and Craig, E. A. (1987) Complex interactions among members of an essential subfamily of hsp70 genes in Saccharomyces cerevisiae. *Mol. Cell. Biol.* **7**, 2568–2577
10. Halliwell, B., Clement, M. V., and Long, L. H. (2000) Hydrogen peroxide in the human body. *FEBS Lett.* **486**, 10–13
11. Tu, B. P., and Weissman, J. S. (2004) Oxidative protein folding in eukaryotes: mechanisms and consequences. *J. Cell Biol.* **164**, 341–346
12. Liguori, I., Russo, G., Curcio, F., Bulli, G., Aran, L., Della-Morte, D., *et al.* (2018) Oxidative stress, aging, and diseases. *Clin. Interv. Aging* **13**, 757–772
13. Gandhi, S., and Abramov, A. Y. (2012) Mechanism of oxidative stress in neurodegeneration. *Oxid. Med. Cell. Longev.* **2012**, 428010
14. Medicherla, B., and Goldberg, A. L. (2008) Heat shock and oxygen radicals stimulate ubiquitin-dependent degradation mainly of newly synthesized proteins. *J. Cell Biol.* **182**, 663–673
15. Reichmann, D., Voth, W., and Jakob, U. (2018) Maintaining a healthy proteome during oxidative stress. *Mol. Cell* **69**, 203–213
16. Hanzén, S., Vielfort, K., Yang, J., Roger, F., Andersson, V., Zamarbide-Forés, S., *et al.* (2016) Lifespan control by redox-dependent recruitment of chaperones to misfolded proteins. *Cell* **166**, 140–151
17. Rhee, S. G., Kang, S. W., Jeong, W., Chang, T. S., Yang, K. S., and Woo, H. A. (2005) Intracellular messenger function of hydrogen peroxide and its regulation by peroxiredoxins. *Curr. Opin. Cell Biol.* **17**, 183–189
18. Winter, J., Linke, K., Jatzek, A., and Jakob, U. (2005) Severe oxidative stress causes inactivation of DnaK and activation of the redox-regulated chaperone Hsp33. *Mol. Cell* **17**, 381–392
19. Delaunay, A., Pflieger, D., Barrault, M. B., Vinh, J., and Toledano, M. B. (2002) A thiol peroxidase is an H2O2 receptor and redox-transducer in gene activation. *Cell* **111**, 471–481
20. Taguchi, K., Motohashi, H., and Yamamoto, M. (2011) Molecular mechanisms of the Keap1-Nrf2 pathway in stress response and cancer evolution. *Genes Cells* **16**, 123–140
21. Suzuki, T., and Yamamoto, M. (2017) Stress-sensing mechanisms and the physiological roles of the Keap1–Nrf2 system during cellular stress. *J. Biol. Chem.* **292**, 16817–16824
22. Santiago, A. M., Gonçalves, D. L., and Morano, K. A. (2020) Mechanisms of sensing and response to proteotoxic stress. *Exp. Cell Res.* **395**, 112240
23. Zhang, H., Gong, W., Wu, S., and Perrett, S. (2022) Hsp70 in redox homeostasis. *Cells* **11**, 829
24. Yang, J., Zhang, H., Gong, W., Liu, Z., Wu, H., Hu, W., *et al.* (2020) S-Glutathionylation of human inducible Hsp70 reveals a regulatory mechanism involving the C-terminal α-helical lid. *J. Biol. Chem.* **295**, 8302–8324

25. Trott, A., West, J. D., Klaić, L., Westerheide, S. D., Silverman, R. B., Morimoto, R. I., *et al.* (2008) Activation of heat shock and antioxidant responses by the natural product celastrol: transcriptional signatures of a thiol-targeted molecule. *Mol. Biol. Cell* **19**, 1104–1112
26. Morano, K. A., Grant, C. M., and Moye-Rowley, W. S. (2012) The response to heat shock and oxidative stress in saccharomyces cerevisiae. *Genetics* **190**, 1157–1195
27. Wang, Y., Gibney, P. A., West, J. D., and Morano, K. A. (2012) The yeast Hsp70 Ssa1 is a sensor for activation of the heat shock response by thiol-reactive compounds. *Mol. Biol. Cell* **23**, 3290–3298
28. Peffer, S., Gonçalves, D., and Morano, K. A. (2019) Regulation of the Hsf1-dependent transcriptome via conserved bipartite contacts with Hsp70 promotes survival in yeast. *J. Biol. Chem.* **294**, 12191–12202
29. Zheng, X., Krakowiak, J., Patel, N., Beyzavi, A., Ezike, J., Khalil, A. S., *et al.* (2016) Dynamic control of Hsf1 during heat shock by a chaperone switch and phosphorylation. *Elife* **5**, e18638
30. Miyata, Y., Rauch, J. N., Jinwal, U. K., Thompson, A. D., Srinivasan, S., Dickey, C. A., *et al.* (2012) Cysteine reactivity distinguishes redox sensing by the heat-inducible and constitutive forms of heat shock protein 70. *Chem. Biol.* **19**, 1391–1399
31. Wang, J., and Sevier, C. S. (2016) Formation and reversibility of BiP protein cysteine oxidation facilitate cell survival during and post oxidative stress. *J. Biol. Chem.* **291**, 7541–7557
32. Xu, M., Marsh, H. M., and Sevier, C. S. (2016) A conserved cysteine within the ATPase domain of the endoplasmic reticulum chaperone BiP is necessary for a complete complement of BiP activities. *J. Mol. Biol.* **428**, 4168–4184
33. Hermawan, A., and Chirico, W. J. (1999) N-ethylmaleimide-modified Hsp70 inhibits protein folding. *Arch. Biochem. Biophys.* **369**, 157–162
34. Liu, Q., Levy, E. J., and Chirico, W. J. (1996) N-ethylmaleimide inactivates a nucleotide-free Hsp70 molecular chaperone. *J. Biol. Chem.* **271**, 29937–29944
35. Nillegoda, N. B., Kirstein, J., Szlachcic, A., Berynskyy, M., Stank, A., Stengel, F., *et al.* (2015) Crucial HSP70 co-chaperone complex unlocks metazoan protein disaggregation. *Nature* **524**, 247–251
36. Zhuravleva, A., and Gierasch, L. M. (2011) Allosteric signal transmission in the nucleotide-binding domain of 70-kDa heat shock protein (Hsp70) molecular chaperones. *Proc. Natl. Acad. Sci. U. S. A.* **108**, 6987–6992
37. Fung, K. L., Hilgenberg, L., Wang, N. M., and Chirico, W. J. (1996) Conformations of the nucleotide and polypeptide binding domains of a cytosolic Hsp70 molecular chaperone are coupled. *J. Biol. Chem.* **271**, 21559–21565
38. Zhu, X. (1996) Structural analysis of substrate binding by the molecular chaperone DnaK. *Science* **5268**, 1606–1614
39. Lum, R., Tkach, J. M., Vierling, E., and Glover, J. R. (2004) Evidence for an unfolding/threading mechanism for protein disaggregation by Saccharomyces cerevisiae Hsp104. *J. Biol. Chem.* **279**, 29139–29146
40. Tkach, J. M., and Glover, J. R. (2004) Amino acid substitutions in the C-terminal AAA+ module of Hsp104 prevent substrate recognition by disrupting oligomerization and cause high temperature inactivation. *J. Biol. Chem.* **279**, 35692–35701
41. Garcia, V. M., Nillegoda, N. B., Bukau, B., and Morano, K. A. (2017) Substrate binding by the yeast Hsp110 nucleotide exchange factor and molecular chaperone Sse1 is not obligate for its biological activities. *Mol. Biol. Cell* **28**, 2066–2075
42. Glover, J. R., and Lindquist, S. (1998) Hsp104, Hsp70, and Hsp40: a novel chaperone system that rescues previously aggregated proteins. *Cell* **94**, 73–82
43. Truman, A. W., Kristjansdottir, K., Wolfgeher, D., Hasin, N., Polier, S., Zhang, H., *et al.* (2012) CDK-dependent Hsp70 phosphorylation controls G1 cyclin abundance and cell-cycle progression. *Cell* **151**, 1308–1318
44. Mumberg, D., Müller, R., and Funk, M. (1995) Yeast vectors for the controlled expression of heterologous proteins in different genetic backgrounds. *Gene* **156**, 119–122
45. Keefer, K. M., and True, H. L. (2017) A toxic imbalance of Hsp70s in Saccharomyces cerevisiae is caused by competition for cofactors. *Mol. Microbiol.* **105**, 860–868
46. Krakowiak, J., Zheng, X., Patel, N., Feder, Z. A., Anandhakumar, J., Valerius, K., *et al.* (2018) Hsf1 and Hsp70 constitute a two-component feedback loop that regulates the yeast heat shock response. *Elife* **7**, e31668
47. Abrams, J. L., Verghese, J., Gibney, P. A., and Morano, K. A. (2014) Hierarchical functional specificity of cytosolic heat shock protein 70 (Hsp70) nucleotide exchange factors in yeast. *J. Biol. Chem.* **289**, 13155–13167
48. Abrams, J. L., and Morano, K. A. (2013) Coupled assays for monitoring protein refolding in Saccharomyces cerevisiae. *J. Vis. Exp.* https://doi.org/10.3791/50432
49. Greene, L., Park, Y.-N., Masison, D., and Eisenberg, E. (2009) Application of GFP-labeling to study prions in yeast. *Protein Pept. Lett.* **16**, 635–641
50. Cohen, A., Ross, L., Nachman, I., and Bar-Nun, S. (2012) Aggregation of PolyQ proteins is increased upon yeast aging and affected by Sir2 and Hsf1: novel quantitative biochemical and microscopic assays. *PLoS One* **7**, e44785
51. Singh, A., Vashistha, N., Heck, J., Tang, X., Wipf, P., Brodsky, J. L., *et al.* (2020) Direct involvement of Hsp70 ATP hydrolysis in Ubr1-dependent quality control. *Mol. Biol. Cell* **31**, 2669–2686
52. Miller, S. B., Ho, C., Winkler, J., Khokhrina, M., Neuner, A., Mohamed, M. Y., *et al.* (2015) Compartment-specific aggregases direct distinct nuclear and cytoplasmic aggregate deposition. *EMBO J.* **34**, 778–797
53. Wang, J., Pareja, K. A., Kaiser, C. A., and Sevier, C. S. (2014) Redox signaling via the molecular chaperone BiP protects cells against endoplasmic reticulum-derived oxidative stress. *Elife* **3**, e03496
54. O'Donnell, J. P., Marsh, H. M., Sondermann, H., and Sevier, C. S. (2018) Disrupted hydrogen-bond network and impaired ATPase activity in an Hsc70 cysteine mutant. *Biochemistry* **57**, 1073–1086
55. Ulrich, K., Schwappach, B., and Jakob, U. (2021) Thiol-based switching mechanisms of stress-sensing chaperones. *Biol. Chem.* **402**, 239–252
56. Picazo, C., and Molin, M. (2021) Impact of hydrogen peroxide on protein synthesis in yeast. *Antioxidants (Basel)* **10**, 952
57. Ahn, S. G., and Thiele, D. J. (2003) Redox regulation of mammalian heat shock factor 1 is essential for Hsp gene activation and protection from stress. *Genes Dev.* **17**, 516–528
58. Marada, A., Allu, P. K., Murari, A., PullaReddy, B. R., Tammineni, P., Thiriveedi, V. R., *et al.* (2013) Mge1, a nucleotide exchange factor of Hsp70, acts as an oxidative sensor to regulate mitochondrial Hsp70 function. *Mol. Biol. Cell* **24**, 692–703
59. Allu, P. K., Marada, A., Boggula, Y., Karri, S., Krishnamoorthy, T., Sepuri, N. B. V., *et al.* (2015) Methionine sulfoxide reductase 2 reversibly regulates Mge1, a cochaperone of mitochondrial Hsp70, during oxidative stress. *Mol. Biol. Cell* **26**, 406–419
60. Karri, S., Singh, S., Paripati, A. K., Marada, A., Krishnamoorthy, T., Guruprasad, L., *et al.* (2019) Adaptation of Mge1 to oxidative stress by local unfolding and altered Interaction with mitochondrial Hsp70 and Mxr2. *Mitochondrion* **46**, 140–148
61. Rahman, I. (2012) Pharmacological antioxidant strategies as therapeutic interventions for COPD. *Biochim. Biophys. Acta Mol. Basis Dis.* **1822**, 714–728
62. Täger, M., Piecyk, A., Köhnlein, T., Thiel, U., Ansorge, S., and Welte, T. (2000) Evidence of a defective thiol status of alveolar macrophages from COPD patients and smokers. Chronic obstructive pulmonary disease. *Free Radic. Biol. Med.* **29**, 1160–1165
63. Liu, X. D., Liu, P. C. C., Santoro, N., and Thiele, D. J. (1997) Conservation of a stress response: human heat shock transcription factors functionally substitute for yeast HSF. *EMBO J.* **16**, 6466–6477
64. Morano, K. A., and Thiele, D. J. (1999) The Sch9 protein kinase regulates Hsp90 chaperone complex signal transduction activity *in vivo*. *EMBO J.* **18**, 5953–5962
65. Andréasson, C., Fiaux, J., Rampelt, H., Mayer, M. P., and Bukau, B. (2008) Hsp110 is a nucleotide-activated exchange factor for Hsp70. *J. Biol. Chem.* **283**, 8877–8884
66. Shaner, L., Sousa, R., and Morano, K. A. (2006) Characterization of Hsp70 binding and nucleotide exchange by the yeast Hsp110 chaperone Sse1. *Biochemistry* **45**, 15075–15084
67. Verghese, J., and Morano, K. A. (2012) A lysine-rich region within fungal BAG domain-containing proteins mediates a novel association with ribosomes. *Eukaryot. Cell* **11**, 1003–1011
68. Ford, A. E., Denicourt, C., and Morano, K. A. (2019) Thiol stress-dependent aggregation of the glycolytic enzyme triose phosphate isomerase in yeast and human cells. *Mol. Biol. Cell* **30**, 554–565